High quantum efficiency long-wave infrared photodiodes using W-structured type-II superlattices

E. H. Aifer[a], C. L. Canedy[a], J. G. Tischler[a], J. H. Warner[a], I. Vurgaftman[a] , W. W. Bewley[a], J. R. Meyer[a] , E. M. Jackson[b], J. C. Kim[a], and L. W. Whitman[a]

[a]Naval Research Laboratory, 4555 Overlook Ave. SW, Washington, DC 20375
[b]SFA Inc., 2200 Defense Hwy, Suite 405, Crofton, MD 21114

Abstract

Recent improvements in material quality and design have led to large improvements in the quantum efficiency (QE) of long-wave infrared (LWIR) photodiodes based on W-structured type-II superlattices (WSL), which now have achieved external QE of up to 35% on an 11.3 μm cutoff photodiode operating at 80K. While single band and dual band WSLs have been demonstrated with cutoff wavelengths out to 17 μm, the initial devices also showed significant losses of photo-excited carriers resulting in QE levels of ≤ 10%. Here we describe recent results in which these losses have been dramatically reduced by modifying the WSL barrier layers to increase the mini-band width and improve the material properties. An additional 35-55% increase in QE also resulted from the use of semi-transparent Te doped n-GaSb substrates that allowed for IR reflections off the backside from the Au plated chip carrier. A series of PIN photodiodes using the improved WSL, with intrinsic regions from 1 to 4 μm thick, were used to study minority carrier transport characteristics in the new structure. As a result of the improved design and material properties, the electron diffusion length in the undoped i-region, as determined from a theoretical fit to the thickness-dependent data, was 3.5μm, allowing for much higher collection efficiency in PIN photodiodes with intrinsic regions up to 4 μm thick.

KEYWORDS: Type-II superlattice, strained layer superlattice, GaSb, III-V, IR detector, LWIR, photodiode

1. INTRODUCTION

W-structured type-II superlattices (WSL), initially developed to increase the gain of mid-wave infrared (MWIR) lasers, are now showing promise for use in long-wave and very-long-wave infrared (LWIR and VLWIR) photodiodes. The WSL was developed by Meyer et al.[1] to address the reduced overlap between conduction and valence states in type-II superlattices, arising from the alternating electron and hole confinement layers. In the WSL, illustrated in Fig. 1, two InAs "electron-wells" are located on either side of an InGaSb "hole-well" and are bound on either side by AlSb (or AlGaInSb) "barrier" layers. The addition of the AlSb layers serves to confine the electron wavefunctions symmetrically about the hole-well, increasing the electron-hole overlap. The characteristically strong absorption of WSLs near the band-edge results mainly from its nearly two-dimensional electron bandstructure.

The use of WSLs in photodiodes was first reported by Fuchs et al.,[2] using structures designed for MWIR laser operation. Mixed results were obtained relative to binary and ternary type-II superlattice (BSL, TSL) photodiodes, with improved optical performance coming at the expense of increased series resistance. Recently, we resumed the investigation of WSL-based photodiodes, extending operation to the LWIR and VLWIR bands[3]. We also began with WSL designs based on lasing applications, using a simple *p-n* photodiode configuration, and found that while the transport results were comparable to those using BSLs and TSLs, quantum efficiencies (QEs) were significantly lower. Transmission measurements indicated that the samples had strong optical absorption, with absorption coefficients of 1600-2000 cm^{-1} within a few microns of the band-edge, indicating that the samples suffered from excess loss of photo-excited carriers.

In this paper we describe a second generation of WSL-based LWIR photodiodes, in which improvements in design, material quality, and the use of semitransparent n-GaSb substrates have strongly reduced the minority carrier losses

Quantum Sensing and Nanophotonic Devices III, edited by Manijeh Razeghi, Gail J. Brown,
Proc. of SPIE Vol. 6127, 61270T, (2006) · 0277-786X/06/$15 · doi: 10.1117/12.660711

Report Documentation Page

Form Approved
OMB No. 0704-0188

1. REPORT DATE	2. REPORT TYPE	3. DATES COVERED
2006		**00-00-2006 to 00-00-2006**

4. TITLE AND SUBTITLE	5a. CONTRACT NUMBER
High quantum efficiency long-wave infrared photodiodes using W-structured type-II superlattices	5b. GRANT NUMBER
	5c. PROGRAM ELEMENT NUMBER
6. AUTHOR(S)	5d. PROJECT NUMBER
	5e. TASK NUMBER
	5f. WORK UNIT NUMBER
7. PERFORMING ORGANIZATION NAME(S) AND ADDRESS(ES) **Naval Research Laboratory,4555 Overlook Avenue SW,Washington,DC,20375**	8. PERFORMING ORGANIZATION REPORT NUMBER
9. SPONSORING/MONITORING AGENCY NAME(S) AND ADDRESS(ES)	10. SPONSOR/MONITOR'S ACRONYM(S)
	11. SPONSOR/MONITOR'S REPORT NUMBER(S)

12. DISTRIBUTION/AVAILABILITY STATEMENT
Approved for public release; distribution unlimited

13. SUPPLEMENTARY NOTES

14. ABSTRACT

Recent improvements in material quality and design have led to large improvements in the quantum efficiency (QE) of long-wave infrared (LWIR) photodiodes based on W-structured type-II superlattices (WSL), which now have achieved external QE of up to 35% on an 11.3 μm cutoff photodiode operating at 80K. While single band and dual band WSLs have been demonstrated with cutoff wavelengths out to 17 μm, the initial devices also showed significant losses of photo-excited carriers resulting in QE levels of ≤ 10%. Here we describe recent results in which these losses have been dramatically reduced by modifying the WSL barrier layers to increase the mini-band width and improve the material properties. An additional 35-55% increase in QE also resulted from the use of semi-transparent Te doped n-GaSb substrates that allowed for IR reflections off the backside from the Au plated chip carrier. A series of PIN photodiodes using the improved WSL, with intrinsic regions from 1 to 4 μm thick, were used to study minority carrier transport characteristics in the new structure. As a result of the improved design and material properties, the electron diffusion length in the undoped i-region, as determined from a theoretical fit to the thickness-dependent data, was 3.5μm, allowing for much higher collection efficiency in PIN photodiodes with intrinsic regions up to 4 μm thick.

15. SUBJECT TERMS

16. SECURITY CLASSIFICATION OF:			17. LIMITATION OF ABSTRACT	18. NUMBER OF PAGES	19a. NAME OF RESPONSIBLE PERSON
a. REPORT	b. ABSTRACT	c. THIS PAGE			
unclassified	**unclassified**	**unclassified**	**Same as Report (SAR)**	**10**	

and resulted in samples with average external QE levels as high as 35%. We present a study in which a series of PIN WSL photodiodes were grown with identical heterostructures, but with intrinsic- (*i*-) region thickness increasing from 1 to 4 μm. From the dependence of QE on i-region thickness, we determine that the minority-carrier electron diffusion length along the growth direction is about 3.5 μm. These results demonstrate that despite the additional complexity of the WSL, including twice as many interfaces per period and reduced electron mobility along the growth axis, WSL photodiodes can provide high QE. With a layer structure optimized for backside-illumination, and with substrate thinning, WSL's can be competitive for focal plane array applications.

2. DESIGN, GROWTH, AND FABRICATION

For this study, a modified WSL heterostructure design with a nominal bandgap of 11.3 μm was developed to address the carrier loss problem by reducing the AlSb barrier height to increase the vertical mobility of minority carrier electrons, and to reduce the Al content in the barrier layer to improve the material properties. To wit, the WSL AlSb barrier layers were replaced with quaternary barrier layers (QBL) consisting of $Al_{0.4}Ga_{0.49}In_{0.11}Sb$. The periodic layer structure is illustrated in Fig. 1, consisting of a 7-mono-layer (ML) thick QBL, two 14-ML-thick InAs electron wells, and one 9-ML-thick $In_{0.19}Ga_{0.81}Sb$ hole well.

Since the conduction band offset of the QBL with respect to the InAs electron well is only 1.3 eV, *vs.* 2.1 eV for AlSb barriers (see Fig. 1), the electron miniband width is nearly doubled in the new design, from 20 to 35 meV. The electron effective mass along the growth direction is thus reduced by 30%, from 0.17 to 0.12 m_0, according to 8-band ***k•p*** calculations. The AlSb content in the QBL is only 40%, with the balance composed of 49% GaSb and 11% InSb. The QBL can thus be grown with excellent structural properties at 430ºC, a temperature compatible with that of the InAs and GaSb layers, and well below that necessary for AlSb, which has an optimal growth temperature over 500°C.[4]

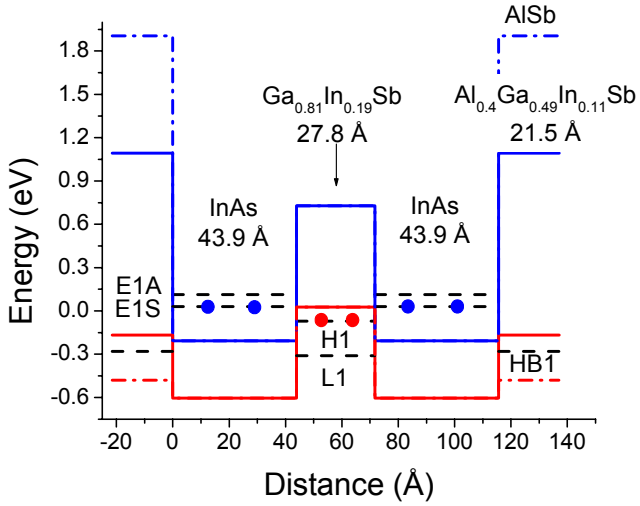

FIG. 1. The WSL band diagram. AlSb barrier layers (dashed) are replaced with QBLs that improve the electron mobility along the growth direction by providing shallower barriers and improved material quality by reducing the Al content by 60%.

The samples were grown in a Riber compact 21T solid-source molecular beam epitaxy system, equipped with a Ga sumo-cell, two In sources and valved As and Sb crackers. For each device-quality wafer, a series of calibration growths were performed with feed back provided by x-ray diffraction (XRD) to measure the strain and periodicity, and photoluminescence (PL) intensity to monitor the overall material quality and bandgap. The PL intensity, which is very sensitive to carrier lifetime and is strongly correlated with QE,[3] has become an integral tool in the characterization of our detector growths, as illustrated in Figure 2. The target structure for the WSL in the present study was lattice matched assuming neutral interfaces, that is, the interface bond composition is expected to contribute no additional strain. The choice of neutral interfaces resulted from a study of PL intensity vs. WSL

interface configuration,[3,5] that linked strong degradation of PL to the use of group-III soaks at the interface transition as a means of forcing InSb or GaAs interface bonds. In reality, cross-sectional scanning tunneling microscopy has revealed that background levels and segregation may still result in a predominant bond type at an interface, such as GaAs bonds at a GaSb/InAs interface under increased As pressure.[6] Nonetheless, the PL data show that group-III soaks are to be avoided. To the extent that background levels and segregation could be eliminated, the nominally lattice matched WSL alloy recipe was typically adjusted in the final calibration growth to minimize strain.

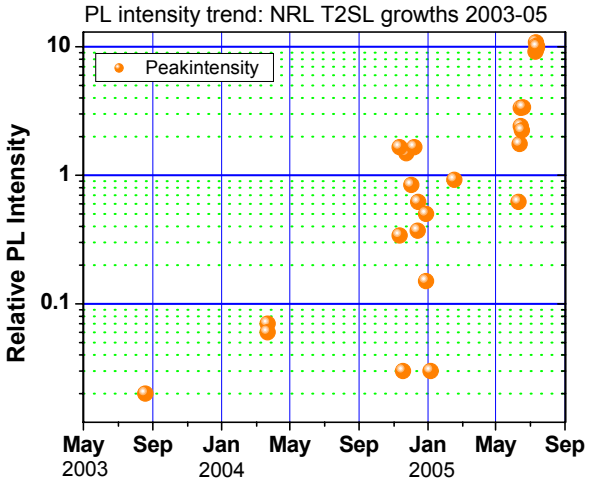

FIG. 2. Relative PL intensity of NRL device wafers over the last 2 years.

A series of 5 WSL PIN photodiodes were grown, all using the WSL (described above) but with undoped *i*-regions of thickness 1, 1.5, 2, 3, and 4 µm. Each PIN diode was grown on an *n*-type (Te doped 1×10^{17} cm^{-3}) GaSb substrate, beginning with a thick *p*+ GaSb contact layer doped with Be to 1-3 $\times$ 10^{18} cm^{-3}, followed by a 0.1-µm-thick p^+-WSL Be-doped to 4×10^{17} cm^{-3}. The undoped *i*-region was grown next, followed by 0.33 µm of n^+-WSL, Si-doped to $4\text{x}10^{17}$ cm^{-3}. The structures were capped with a 10-nm-thick n^+-InAs contact layer, also Si-doped to $4\text{x}10^{17}$ cm^{-3}. While final adjustments in the alloy recipe resulted in wafers with negligible strain (120 ppm maximum, < 50 ppm typical, as shown in Fig. 3) and high PL intensity, the superlattice period was allowed to vary by as much as 5% (2 ML), resulting in cutoff wavelengths ranging from 9.3 to 11.3 µm.

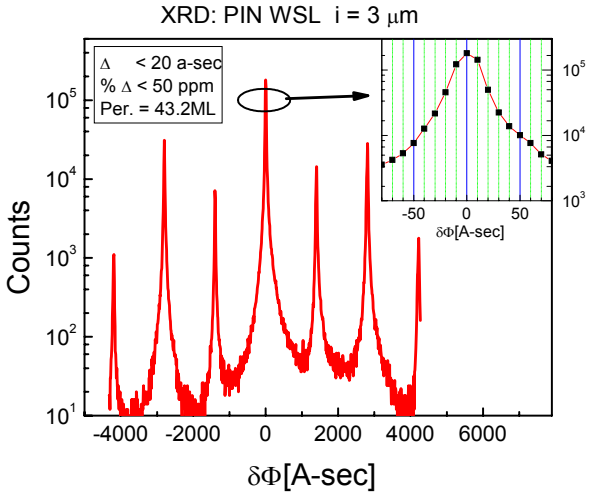

FIG. 3. XRD spectrum of a PIN WSL photodiode with 3-µm-thick *i*-region, indicating negligible strain.

Unpassivated, circular mesa diodes, of 100 to 400 μm diameter, were fabricated using a 2-step wet-etch based process. First, lithographically defined mesas are isolated by etching 1.5 to 4.5 μm through the superlattice, down to the p^+-GaSb contact layer. The devices are then completed by depositing Ti / Pt /Au Ohmic contacts on both the n^+-InAs cap layer and the p^+ GaSb bottom contact layer exposed at the base of the mesas. Optical access to the top-illuminated photodiodes was provided by windowed and small circular dot "contacts" (Fig. 4). Dies were then packaged in standard 68-pin LCC chip carriers and electrically connected by Au-ball-bonding at low force (< 40 gm) directly to contacts on the top and at the base of the mesas.

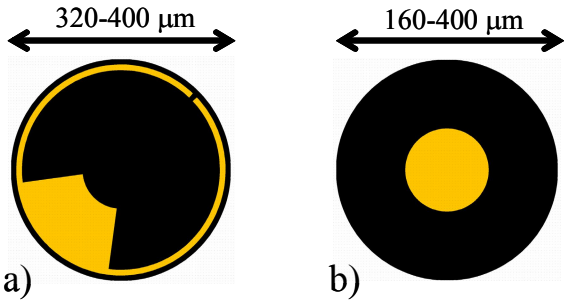

FIG. 4. Window (a), and "dot" (b) contacts on top-illuminated photodiodes, arranged for wirebonding directly to mesas.

3. RESULTS AND DISCUSSION

External Quantum efficiencies were measured using a calibrated blackbody operating at a temperature of 1000K. The IR flux was chopped at 37 Hz, and was incident on the device under test through a narrow band-pass filter centered at 5.34 μm with a 0.35 μm FWHM. The average QE within the filter pass-band was determined from the ratio of detector photocurrent to the blackbody flux measured using a calibrated Optronics Laboratories 740-17C pyrometer. This value was then used to rescale the normalized QE spectra obtained from the photodiode response, measured using a Fourier transform infrared spectrometer. Independent QE measurements were also performed on several of the samples in this study at Rockwell Scientific Co. and at Northwestern University. Results are given in Fig. 5 for the 2, 3 and 4 μm thick *i*-region samples respectively. The average external QE is seen to increase steadily with *i*-region thickness, up to a value of about 35% for the 4-μm-thick *i*-region device (measured within 25% of the cutoff wavelength), which is among the highest published for a type-II superlattice.[7,8] Transport properties were also measured, yielding average dynamic-impedance-area product (R_0A) values of 10-20 Ohm-cm^2 at 80 K, which are comparable to the best previous type-II values,[9] but are about a factor of 10 lower than the state of the art for MCT in this wavelength range.

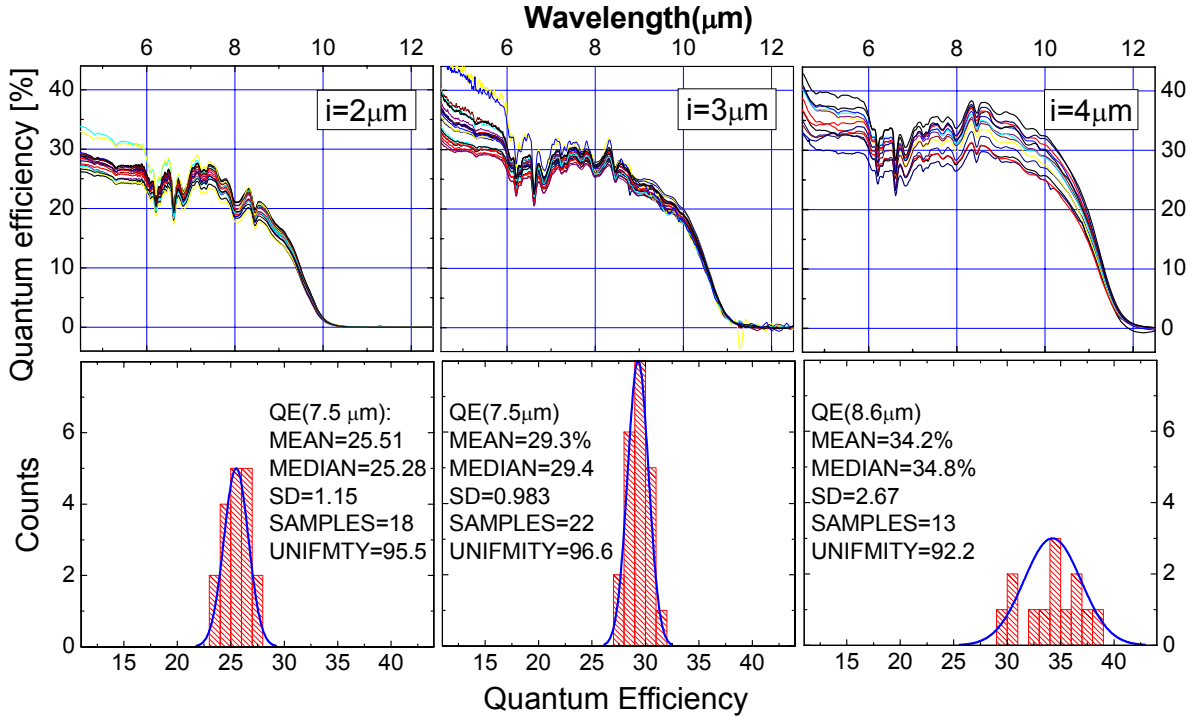

FIG. 5. Quantum efficiency spectra for PIN WSL photodiodes at 80K with 1, 2, and 4 μm thick intrinsic regions.

In PIN photodiodes, the QE is largely determined by three factors: the absorption coefficient, the background impurity concentration in the *i*-region (N_{bgnd}), and the minority carrier diffusion length (L_n). While the absorption coefficient determines the rate of optical generation, N_{bgnd} and L_n determine the volume of the semiconductor over which photo-excited carriers can contribute significant photocurrent, through drift or diffusion processes respectively.

In an ideal PIN diode, the background impurity concentration is negligible and an electric field extends across the *i*-region, sweeping all photo-excited carriers across the junction. If the residual doping levels are appreciable however, the field is restricted to a relatively short depletion region, so that most photo-excited carriers must diffuse a significant distance across the quasi-neutral *i*-region to be collected. In this case, the minority carrier diffusion length is a critical factor in determining the detector quantum efficiency.

This behavior can be understood from Hovel's expression[10] for quantum efficiency in a *p*-*n* junction, shown below, where we have set the surface recombination velocity to 0. The total QE is the sum of contributions from three regions: $QE = QE_{pn} + QE_{SCR} + QE_{np}$. In the space charge region, $QE_{SCR} = (1-R)\left[e^{-\alpha x_n} - e^{-\alpha x_p}\right]$, and it depends only on the reflectivity of the top surface $\boldsymbol{R}$, the absorption coefficient $\boldsymbol{\alpha}$, and on $\boldsymbol{N_{bgnd}}$ through the boundaries of the *n* and *p* depletion regions $\boldsymbol{x_n}$, and $\boldsymbol{x_p}$. The collection of minority electrons from the quasi-neutral *p*-region, however, is a strong function of the electron diffusion length ($\boldsymbol{L_n}$), and its ratio with respect to the length of the diode, $\frac{W_H}{L_n}$,

$$QE_{np} = (1-R)\frac{\alpha L_n}{(\alpha L_n)^2 - 1} e^{-\alpha x_p} \left[\alpha L_n - \frac{\sinh\left(\frac{W_H}{L_n}\right) + \alpha L_n e^{-\alpha W_H}}{\cosh\left(\frac{W_H}{L_n}\right)} \right].$$

Similarly for the quasi-neutral *n*-region, the contribution from photo-excited holes is

$$QE_{pn} = (1-R)\frac{\alpha L_p}{(\alpha L_p)^2 - 1} \left[\frac{\alpha L_p - e^{-\alpha x_n} \sinh\left(\frac{x_n}{L_p}\right)}{\cosh\left(\frac{x_n}{L_p}\right)} - \alpha L_p e^{-\alpha x_n} \right],$$

where $\boldsymbol{L_p}$ is the diffusion length for holes. However, this contribution is negligible owing to the thinness of the layer, the high doping, and the very low mobility of the minority holes.

These expressions can be used to obtain a lower bound for the electron diffusion length, provided the background carrier concentration, $\boldsymbol{N_{bgnd}}$ is known. For this purpose, an undoped WSL Hall sample was prepared, in which a 1-μm-thick $AlAs_{0.4}Sb_{0.92}$ lattice-matched insulating layer was grown to isolate the 2-μm-thick undoped WSL from the conductive *n*-GaSb substrate. The structure was capped with a 10-nm-thick n^+-InAs contact layer identical to that used for the photodiodes. Greek-cross van de Pauw structures were lithographically patterned and wet-etched, and Ti/ Pt /Au Ohmic contacts deposited to assure symmetric Hall geometry and contact integrity. As a last step, a shallow wet etch was performed masked only by the contacts, to remove the n^+-InAs contact layer from the test structure. Hall measurements were carried out using a swept magnetic field from 0 to 9 Tesla, and the longitudinal and transverse conductivities as a function of field were fit using the multi-carrier quantitative mobility spectrum analysis (QMSA).[11] The results for measurements over the temperature range 40-250K are shown in Fig 6. QMSA shows two sets of carriers present. For temperatures below 200K, a residual hole density (half-circles) is evident, that is nearly independent of temperature down to 40K, with an average value of about 2×10^{15} cm^{-3} and a constant mobility of ≈ 4500 cm^2/V-sec. Above 170K, both holes and electrons (solid circles) are thermally activated, with the electron mobility between 11,000 and 14,000 cm^2/Vs. The electron density crosses over that of the holes just above 170K, where the raw single-field data (at B= 2 Tesla) show the Hall coefficient to become *n*-type. In the inset to Fig. 6, we fit the slope of the log plot of $\frac{np}{T^3} \propto \exp\left(-\frac{E_G}{k_B T}\right)$ *vs.* 1000/T, at high temperature to obtain the energy gap E_G = 121 meV, which agrees well with the PL peak for this sample.

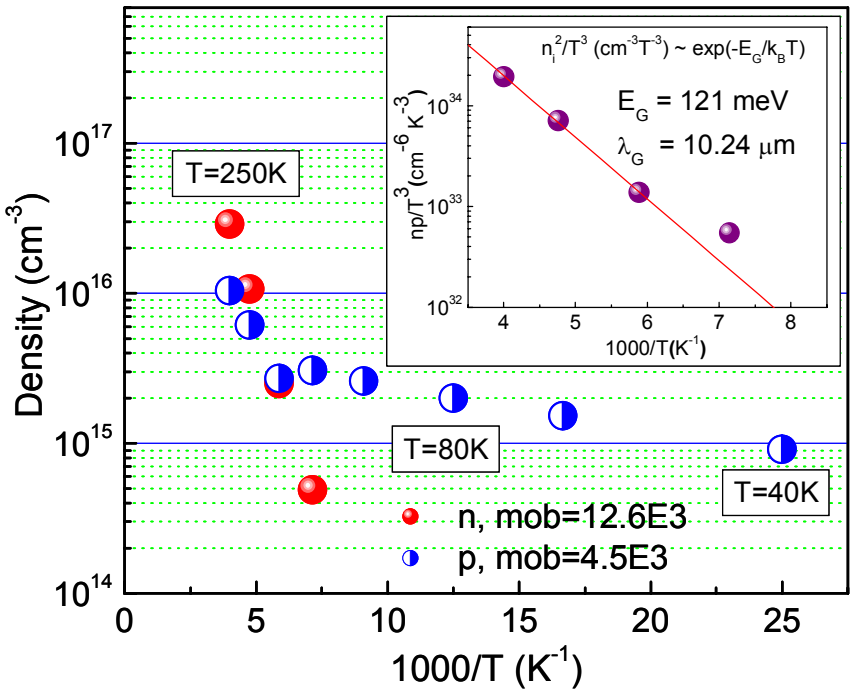

FIG. 6. QMSA fit to the swept-field Hall data for the WSL test structure. The data show a 2×10^{15} cm^{-3} *p*-type background impurity concentration in the nominal "*i*"-region. Inset: Fit of np/T^3 vs $1000/T$, which yields E_G=121 meV.

Using a p-type background concentration of 2×10^{15} cm^{-3} at 80K, and an effective single-pass absorption coefficient of 2200 cm^{-1}, we simulated the measured QE at 80K with the electron diffusion length as a parameter (Fig. 7). Other fixed parameters include the hole diffusion length, L_p =0.5 μm, the WSL dielectric constant ε_w=12.25 ε_0, and density-of-states hole and electron effective-masses of 0.4 and 0.04, respectively. With surface recombination velocities set to zero, the fit provides a lower-bound estimate of L_n=3.5 μm for the electron diffusion length in the WSLs used in this study.

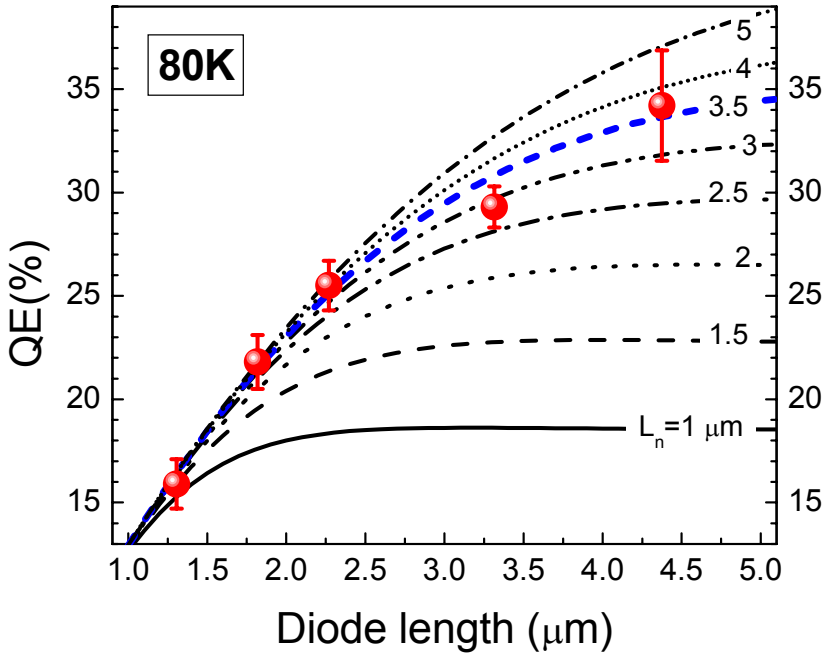

FIG 7. PIN WSL results fit with electron diffusion length as a parameter.

One remaining issue is that the lineshapes exhibited in Fig. 5 are atypical of the WSL spectra expected from the absorption measurements, since they lack the characteristic peak near cutoff, and also exhibit sharp, oscillatory features that are fixed in pattern. As can be seen in Fig. 8, the additional structure corresponds to features in the transmission spectrum of the metal-filled epoxy used to bond the samples to the gold plated chip carriers.

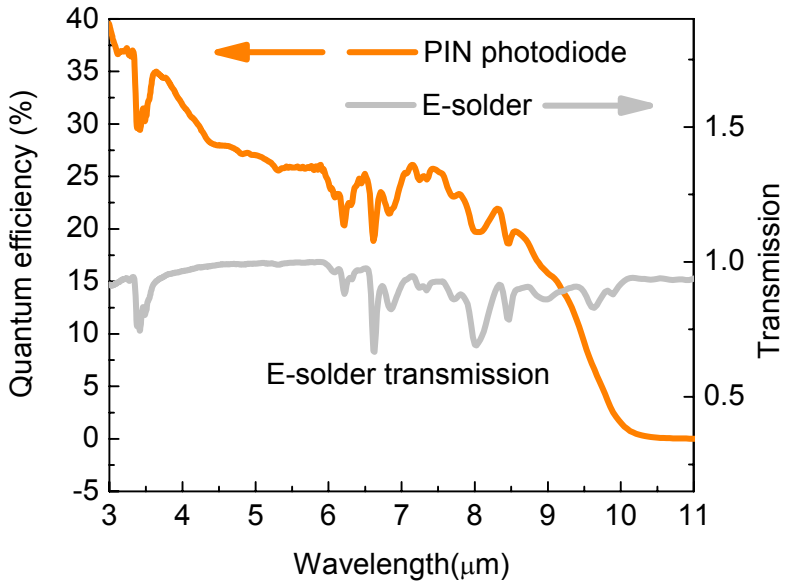

FIG 8. QE spectrum of WSL PIN photodiode with 2μm-thick i-region compared with transmission spectra of E-solder, a metal filled epoxy used to mount the samples to the Au plated chip carrier chip-well.

Evidently, light passing through the 500-µm-thick *n*-GaSb substrate is reflecting off the backside and is contributing to photo-generation. Based on transmission measurements of the WSLs on thinned n-GaSb substrates, and on separate p-GaSb and E-solder samples, we estimate that multiple internal reflections enhance the measured QE over the single pass value by 55% for the 1µm- to 35% for the 4 µm-thick i-region sample. This effect results in a further underestimation of the diffusion length, since the relative increase in QE due to reflections increases as the strongly absorbing i-region thickness decreases. In figure 9, we compare the QE spectra of a WSL PIN diode with a 2 µm-thick i-region grown on a semi-transparent n-GaSb substrate with that of a similar structure grown on an absorbing p-GaSb substrate (the spectrum is shifted in wavelength for better alignment). With multiple reflections, it can be seen that in addition to changes in line-shape, peak QE is enhanced by about 50% over the single pass value represented by the spectrum of the sample with the opaque substrate.

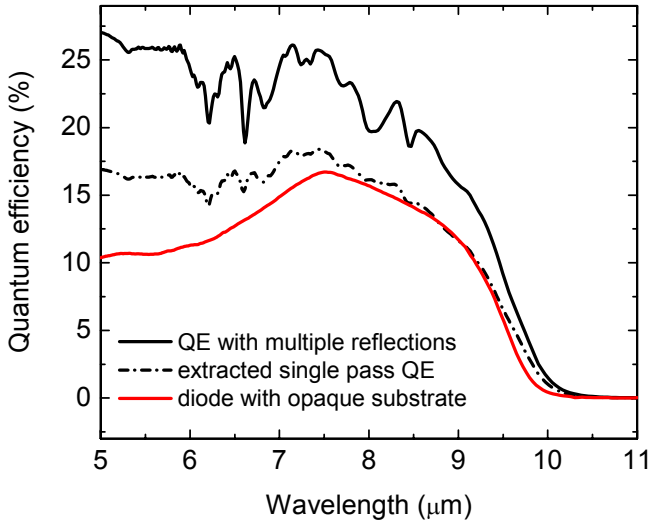

FIG 9. Comparison of measured QE spectra for sample with semi-transparent (n-GaSb, $N_d=10^{17}cm^{-3}$) substrate having multiple internal reflections (solid black line) and sample with opaque substrate (p-GaSb, $N_a=1.4\cdot10^{17}cm^{-3}$) (shifted to align in wavelength). Dashed line is extracted single pass QE for sample with transparent n-GaSb substrate.

The dashed curve is obtained from the multiple-reflection QE-spectrum (QE_{MP}) by summing the internal reflections and extracting the single pass QE (QE_{SP}) as indicated in Fig. 10, where $\boldsymbol{w_{n,i,p}}$ are the WSL transmission spectra for the n-, i- and p-regions, and $\boldsymbol{p}$, $\boldsymbol{S_n}$, and $\boldsymbol{E}$ are those for the p-contact, the substrate, and the E-solder respectively. The summation includes reflections only off the top and bottom surfaces, using constant (independent of wavelength) reflection coefficients $\boldsymbol{R_W}$ and $\boldsymbol{R_c}$ respectively, while the full spectra are used for the transmission terms.

$$I=\sum_{n=0}^{\infty} I_n^+ + I_n^- = I_0(1-R_w)\cdot\left(\frac{1+\beta^-}{1-\beta^+}\right)$$

$$\beta^+ \equiv (w_n w_i w_p p S_n E)^2 R_W R_c \qquad \beta^- \equiv \frac{\beta^+}{w_i w_n^2 R_W}$$

$$QE_{MP}=\left(\frac{1+\beta^-}{1-\beta^+}\right)\cdot QE_{SP}$$

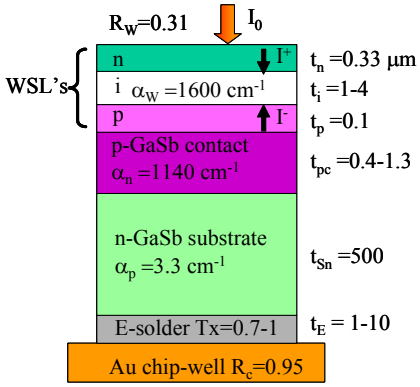

FIG 10. Algorithm for extracting single pass QE spectrum from measured QE. Parameter values are for λ=7.5 µm.

4. CONCLUSION

A study of WSL PIN photodiodes was presented, in which the dependence of quantum efficiency on intrinsic-region thickness was investigated. Combining these results with Hall measurements on a similarly-grown undoped WSL test structure, in which a 2×10^{15} cm^{-3} *p*-type background was measured, an estimate for the vertical minority-carrier diffusion length can be extracted. It was thus determined that the WSL PIN photodiodes, with external QE of up to 35%, have diffusion lengths of ≥ 3.5 μm. That value gives a measure of WSL material quality, and also provides a key input for PIN WSL designs.

The authors gratefully acknowledge Dr Manijeh Razeghi and her students at Northwestern University, and Dr Gerald Sullivan, Gernot Hildebrandt, and Dr. Mark Fields at Rockwell Scientific Co. for confirming several of the QE results in this paper. This work was supported by the Office of Naval Research.

References

1. J. R. Meyer, C. A. Hoffman, F. J. Bartoli, and L. R. Ram-Mohan, *Appl. Phys. Lett*. **67**, 757 (1995).
2. F. Fuchs, L. Burkle, R. Hamid, N. Herres, W. Pletschen, R. E. Sah, R. Kiefer, J. Schmitz, Proc. SPIE **4288**, 171-82, (2001).
3. E. H. Aifer, J. G. Tischler, J. H. Warner, I. Vurgaftman, J. C. Kim, J. R. Meyer, B. R. Bennett, L. W. Whitman, E. M. Jackson, and J. R. Lorentzen, *Proc. SPIE* **5732**, 259-272 (2005).
4. G. I. Boishin, C. L. Canedy, I. Vurgaftman, J. R. Meyer, and L. J. Whitman *J. Cryst. Growth.* **286**, 32 (2006), *in press.*
5. C. L. Canedy, W. W. Bewley, C. S. Kim, M. Kim, I. Vurgaftman, and J. R. Meyer, *J. Appl. Phys.* **94**, 1347 (2003).
6. E. M. Jackson, G. Boishin, E. H. Aifer, B. R. Bennett, and L. W. Whitman, *J. Cryst. Growth* **270/3-4**, 301 (2004).
7. Y. Wei, A. Gin, and M. Razeghi, Appl. Phys. Lett. **80**, 3262 (2002)
8. Y. Wei, A. Hood, V. Yazdanpanah, M. Razeghi, M. Z. Tidrow, and V. Nathan, Appl. Phys. Lett. **86**, 091109 (2005).
9. R. Rehm, M. Walther, F. Fuchs, J. Schmitz, and J. Fleissner, Appl. Phys. Lett. 86, 173501 (2005).
10. H. J. Hovel, Semiconductors and Semimetals Vol. 11, (Academic Press, New York, 1975), pp. 17-20.
11. I. Vurgaftman, J. R. Meyer, C. A. Hoffman, D. Redfern, J. Antoszewski, and L. Faraone, J. Appl. Phys. 84, 4966 (1998).